

PART 3: Volcanic eruptions and associated products

CHAPTER 4.4 Pyroclastic Density Currents

Charbonnier, S.J.¹, Breard, E.C.P.², Engwell, S.³, Roche, O.⁴, Báez, W.A.⁵, Belousova, M.⁶,
Brand, B.⁷, Lerner, G.A.⁸, Ogburn, S.E.⁹

¹ School of Geosciences, University of South Florida, Tampa, FL, USA

² School of Geosciences, The University of Edinburgh, Edinburgh, United Kingdom

³ British Geological Survey, Edinburgh, United Kingdom

⁴ Laboratoire Magmas et Volcans, IRD, Université Clermont Auvergne, Clermont-Ferrand, France

⁵ Universidad Nacional de Salta- CONICET, Salta, Argentina

⁶ Institute of Volcanology and Seismology, Kamchatsky, Russia

⁷ Department of Geosciences, Boise State University, Boise, ID, USA

⁸ División de Geociencias Aplicadas, Instituto Potosino de Investigación Científica y Tecnológica (IPICYT), San Luis Potosí, Mexico

⁹ U.S. Geological Survey Volcano Disaster Assistance Program, Cascades Volcano Observatory, Vancouver, WA, USA

Abstract

Pyroclastic density currents (PDCs) are hot mixtures of gases and volcanic rock of diverse size, nature, or density, capable of flowing over long distances at velocities of tens to hundreds of kilometers per hour. They typically originate from the gravitational collapse of explosive eruption columns, lava domes or lava-flow fronts, unstable upper-flank material or from explosive lateral blasts. PDCs are produced from volcanic eruptions across many orders of magnitude in size and remain one of the deadliest volcanic hazards. In the last decade, significant progress in understanding PDC internal dynamics and associated hazards has been made thanks to major advances in numerical modeling and experimental studies. This chapter outlines what is known about the nature and behavior of PDCs based on observations, experiments, theory, and models; briefly reviews the main approaches used to characterize PDCs and their deposits; and finally highlights recent advances that constrain, test and enhance PDC models.

Keywords: Pyroclastic density currents, internal flow dynamics, deposit characteristics, experiments, numerical models

1. Introduction

Pyroclastic density currents (PDCs) are complex volcanic flows whose occurrence, dynamics and flow paths are often unpredictable, making them a significant threat to human infrastructure and populations surrounding volcanic edifices [1]. They consist of hot (typically between 100 and 850°C) mixtures of gases and particles (volcanic rocks of diverse size, nature, or density), capable of flowing over long distances (a few to many tens of kilometers from the source) and at high velocities (tens to hundreds of kilometers per hour) (e.g., [E1,2]). Typically, PDCs originate from the gravitational collapse of explosive eruption columns, collapse of lava domes or lava-flow fronts, unstable upper-flank material or from explosive lateral blasts. Volcanic eruptions across many orders of magnitude, from small-volume events (<0.001 to 1 km^3) to large-volume caldera-forming eruptions (10^1 – 10^3 km^3 , e.g., [E1,2]) produce PDCs. Since 1500 AD, PDCs have been the deadliest of all volcanic hazards: 60,473 fatalities (including 515 since the 59,958 fatalities published by [1] in 2017) were caused directly by PDCs. Within 10 km and 20 km of a volcano, 90% and 50% of PDC fatalities, respectively, were recorded [1].

Sedimentological and physical models of PDCs have been the subject of numerous studies over the last fifty years or so, summarized in various literature reviews (e.g., [2-5]). In the last decade, significant progress in understanding PDC processes has been made thanks to major advances in numerical modeling and experimental studies. As of today, PDCs can be conceptualized as a particulate flow, depth-organized in a continuum of volumetric particle concentration, ranging from a concentrated basal layer (concentration $>30 \text{ vol.}\%$, usually 30 – $75 \text{ vol.}\%$) named here the **concentrated basal underflow** (which has its own momentum), to a more dilute ($>\sim 0.01 \text{ vol.}\%$) upper layer that is vertically density stratified and referred to here as the upper ash-cloud surge (ACS). The **upper ash-cloud surge** transitions into a buoyant thermal layer (co-PDC plume) when concentrations locally reach $<\sim 0.01 \text{ vol.}\%$, making PDCs strongly non-uniform in depth. Both

54 the concentrated basal underflow and the upper ash-cloud surge layers may be thermally and/or
55 kinematically coupled or behave independently, depending on the concentration gradient (e.g.,
56 [4]) ([Fig. 1](#)).

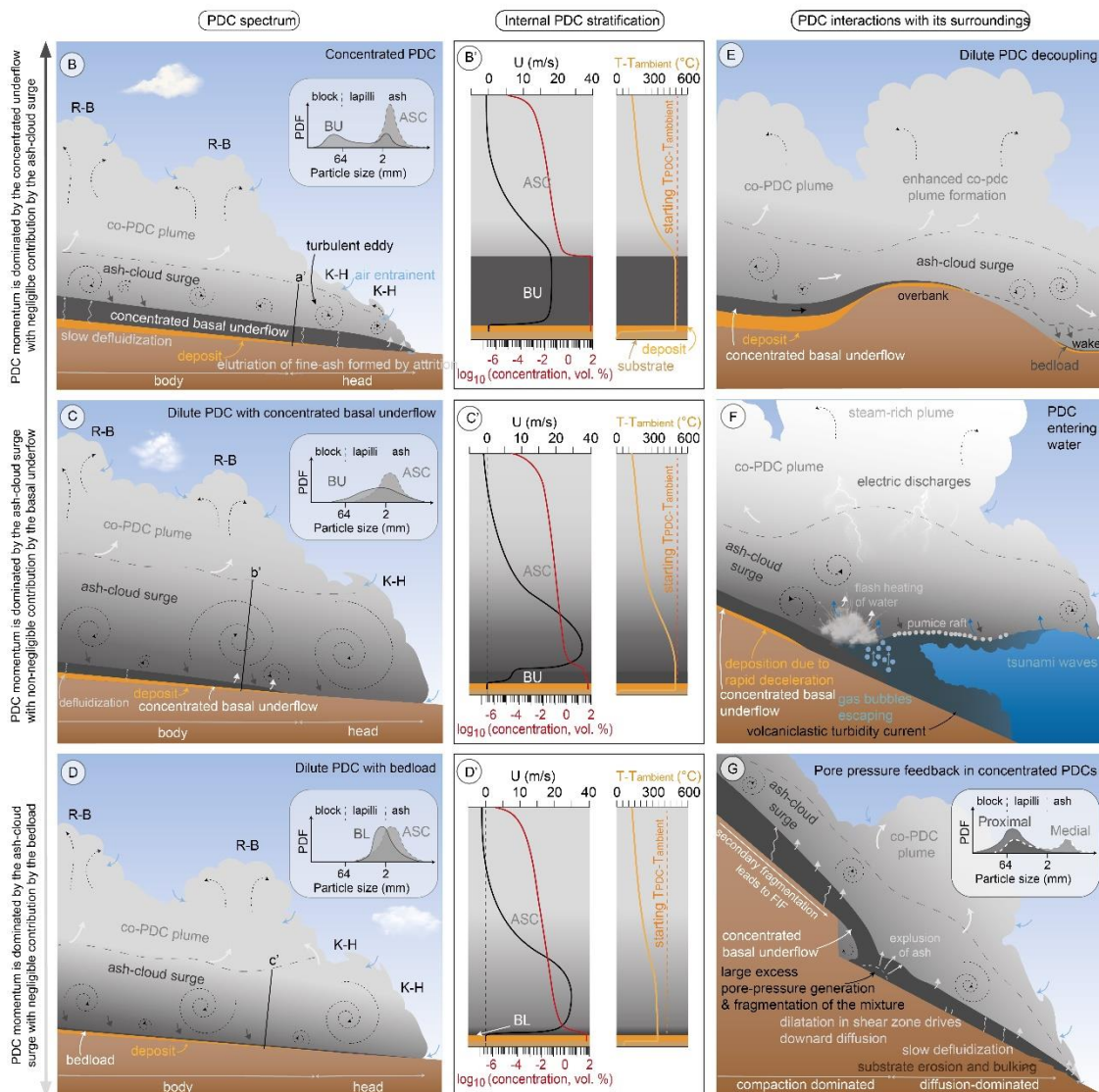


Figure 1: A: Picture of a pyroclastic density current (PDC) at Volcán de Fuego (Guatemala) formed by oversteepened volcanoclastic collapse on September 13, 2012 (Note the picture was flipped; credit: Vinicio Bejarano). **B-G:** Sketch of PDC spectrum and internal structure of the flow (using concentration, velocity and temperature profiles of the mixture), spanning concentrated PDC (B, B'), dilute PDC with concentrated underflow (C, C') and dilute PDC with bedload (D, D'). Common PDC interactions and effect on the flow structure are shown for a PDC interacting with a hill (E), a PDC entering water (F) and a PDC going over a topographic step (G). A key at the bottom explains the acronyms and meaning of arrows that reflect the motion of gas, sedimentation or turbulent eddies. In subpanels B, C, D and G, time- and depth-averaged grain-size distributions transported in the upper ash-cloud surge (ACS) and concentrated underflow (BU) and bedload (BL) are illustrated. Note that in panel **B'**, **C'** and **D'**, the vertical orange line represents the temperature of the PDC at its initiation (differences from the baseline are a consequence of cooling through ambient air entrainment and internal mixing). PDF: Probability Density Function.

There is growing agreement in the PDC research community that **micro-to-mesoscale heterogeneities** (on length-scales of 10^{-6} – 1 m) in grain size, density, and packing within the flowing material develop during emplacement and are key to shaping the overall flow behavior, particularly in the concentrated regime. Such small-scale variations can influence the flow's **large-scale dynamics**, driving unsteady behavior at both the **macro-scale** (1 – 10^2 m) and the **flow-scale** (10^2 – 10^5 m) [3]. Additionally, they contribute to the distinct behavior observed between different regions of the flow [5]. While this general conceptual model seems commonly accepted by the community, the physical behavior of these separate flow regions is still debated today (e.g., [4]).

The purpose of this chapter is to first summarize what is known about the nature and behavior of PDCs based on observations, experiments, theory and models. We then briefly review the main approaches used to characterize PDCs and their deposits. Finally, we outline recent advances that aim to constrain, test, and enhance experimental and numerical models of PDCs in order to develop robust hazard models that can reliably assist risk mitigation.

2. PDCs and their deposits

2.1. Generation, transport, and deposition of PDCs

2.1a. Generation mechanisms

[Table 1](#) shows a classification of PDCs according to historically used flow names and generation mechanisms. It is important to note, however, that flows exist on a continuum between these endmembers. Individual flows may transition in concentration and behavior both spatially and temporally, and PDCs generated by a given mechanism may differ in flow concentration. [Table 1](#) gives a general description of these flow types and their deposits, while additional information about PDC deposits can be found in section 2.2a.

Column-collapse PDCs are generated during explosive eruptions that produce vertical columns that fail to remain fully buoyant. Column-collapses during phreatomagmatic eruptions produce PDCs that can be relatively wet and cool (base or wet surges). Sustained collapses of Plinian eruption columns during caldera-forming eruptions produce voluminous ignimbrite deposits that blanket the landscape (caldera-forming PDCs). In some cases, tall vertical columns may not fully develop and instead collapse just above the vent, resulting in “boil-over” PDCs.

Dome-collapse PDCs are generated by the explosive [E2, E3] or gravitational collapse of lava domes [E2]; lava flow front PDCs are generated by collapse of lava flow fronts ([Table 1](#)). Gravitational dome collapse largely occurs due to oversteepening of dome margins, increased loading on support structures, or removal of support. It can be triggered by rapid dome extrusion; slumping of underlying talus; changes in dome extrusion direction or the extrusion of new lobes; extreme rainfall entering cracks; or, in the case of inactive domes, hydrothermal alteration weakening the dome. Gas over-pressurization of domes can lead to auto-brecciation, and collapse and retrogressive failures can occur where successive collapses eventually undermine or expose a pressurized dome core, leading to large scale collapse and PDC generation. Dome collapses are also triggered by explosions, with many volcanoes experiencing cyclic transitions between explosive and effusive activity [E3]. Lateral or directed blasts through a lava dome or cryptodome involve rapid decompression of the dome and unroofing of the conduit and can

produce highly erosive PDCs that travel great distances. During the flow of any type of PDC, parts of the parent flow can overbank channels or become detached from the parent flow and travel in unexpected directions.

Other less frequent PDC generation mechanisms are discussed in Table 1 and include the collapse of accumulated pyroclastic ejecta (accumulate-collapse PDCs), rapid sedimentation from parent PDCs traversing steep slopes (surge-derived PDCs), post-emplacement avalanching of deposits (deposit-derived or secondary PDCs), and interactions between PDCs, snow, and ice (volcanic mixed avalanches).

120 **Table 1:** Classification of pyroclastic density currents (PDCs) according to general flow name and generation mechanism.

Flow name(s)	Generation mechanism	Description	Examples
Column-collapse PDC, pumice flow, nuées ardentes d'explosions vulcaniennes, St. Vincent-type	Partial collapse of a vertical Vulcanian or sub-Plinian explosion column	These flows produce unwelded pumice-and-ash deposits that may contain disrupted dome material; flow direction may be radially- distributed or influenced by wind or summit topography	Soufrière St. Vincent, Saint Vincent and the Grenadines, 1979; Lascar, Chile, 1993
Boil-over column-collapse PDC	Low pyroclastic fountaining or “boil-over” column-collapse	Unlike a typical column-collapse PDC, a buoyant plume does not develop and instead collapses just above the vent, resembling a pot “boiling over” and generating radially distributed PDCs, which may be concentrated or more dilute, and which have limited or no associated tephra-fall deposits	Lamington, Papua New Guinea, 1951; Tungurahua, Ecuador, 2006
Dome-collapse PDC, block-and-ash flow, nuées ardentes d'avalanche, Merapi-type	Explosive or gravitational collapse of a lava dome	Often partitioned into a concentrated basal underflow and an upper ash-cloud surge, these flows produce block-and-ash deposits, strongly controlled by topography and often confined to a few drainages in the direction of the collapse	Merapi, Indonesia, 2006; Unzendake, Japan, 1991; Soufrière Hills, Montserrat, 1996
Lava-flow-front-collapse PDCs, block-and-ash flow, nuées ardentes d'avalanche, Merapi-type	Collapse of a lava flow front	Similar to dome-collapse PDCs, but involve the collapse of the front of a lava flow rather than a dome and are usually relatively smaller volume	Merapi, Indonesia, 25 April 2006; Santa María (Santiaguito), Guatemala, 1982, November 2002
Accumulate-collapse PDC, oversteepened volcanoclastic collapse PDC	Collapse of accumulated ejecta and volcanoclastic material from the crater rim or upper flanks	Often occurring during eruptions with lava fountaining or ejection of incandescent debris, these flows are formed by the gravitational collapse of hot pyroclastic debris (bombs, scoria,	Tungurahua, Ecuador, February 2010; Pavlof, USA, 2013-2014; Stromboli, Italy, 1930, 2021-2022; Fuego, Guatemala, 2018

		lava spatter, tephra) accumulated on and around volcanic summits	
Overbank and detached PDCs	Overspill of the concentrated basal underflow (\pm ash-cloud surge) of a channelized PDC or detachment of the ash-cloud surge from the channelized concentrated basal underflow	Overspill and detachment are typically caused by changes in topography (e.g., channel constrictions and bends, slope changes) and changes in flow characteristics (e.g., mass flux). Overbank PDCs and detached ash-cloud surges are responsible for many fatalities due to their unpredictable flow directions and ability to reach areas far outside flow channels.	Soufrière Hills, Montserrat, 1997; Merapi, Indonesia 2010;
Lateral or directed blast PDC, nuées peléennes d'explosion dirigée, Pelée-type	Lateral or directed blast through a lava dome or cryptodome, triggered by rapid decompression	These PDCs can rapidly travel great distances due to the initial blast component, are highly erosive, and produce complex deposits, often containing entrained material	Pelée, Martinique, 1902; Bezymianny, Russia 1956; Mount St. Helens, USA, 1980
Caldera-forming PDCs, ash flow, VTTS-type, Valles-type	Sustained collapse of a Plinian eruption column, explosive caldera formation	These large volume PDCs produce voluminous, sheet-like, unwelded to highly welded ignimbrites or ash-flow tuff deposits; these flows may travel over water for considerable distances	Novarupta, USA, 1912; Valles Caldera (Bandelier Tuff), USA, Pleistocene; Taupo, New Zealand, 1800 years BP, Campanian Ignimbrite, Italy, 38.8 ka
Pyroclastic surge, base surge, wet surge, ground surge, Surtseyan-type	Collapse of eruption column, commonly, but not always, derived from a phreatomagmatic eruption	Dilute, turbulent PDC often produced by collapse of a phreatomagmatic eruption column or dilute, turbulent end-member of directed-blast PDCs	Taal, Philippines, 1965; Fayal, Azores (Portugal), 1957; Vestmannaeyjar (Surtsey), Iceland, 1963
Surge-derived PDC, derivative pyroclastic flow	Rapid sedimentation from parent PDCs when the parent flow escapes valley-confines or traverses steep slopes	These flows are more mobile than the parent flow, can travel quite far, sometimes in different directions than that of the parent flow, and generate fine-grained deposits	Soufrière Hills, Montserrat, 25 June 1997, 26 December 1997; Mount St. Helens, USA, 18 May 1980

Secondary PDC, deposit-derived PDC	Post-emplacement avalanching of parent PDC deposit	Caused by post-emplacement avalanching of a parent flow deposit, these flows can occur several years after initial emplacement, are massive and valley-filling, are often fines-depleted compared to the parent flow, and may include an avalanche scarp	Pinatubo, Philippines, 1991-1993
Volcanic mixed avalanche, volcanic ice-slurry flow, hybrid flow	PDC (of any type) interacting with and entraining snow or ice	These flows are caused by PDCs traveling over snow- or ice-clad summits, entraining meltwater and ice blocks, and sometimes transforming into lahars downslope	Redoubt, USA, 1989; Augustine, USA, 2006; Llaima, Chile, 2008

121

2.1b. Internal structure

The internal structure of a PDC is governed by processes that operate across a wide range of scales, from individual particle interactions with the substrate to large-scale obstacles. Since the sizes of particles span orders of magnitude, *gas-particle coupling* occurs over a wide range of regimes. An important scaling parameter for gas-particle coupling in a current with characteristic length scale L and velocity scale U is the Stokes number. It is defined as the ratio of the characteristic particle momentum response time, τ_p , to the characteristic flow time, $\tau_f=L/U$, with

$$\tau_p = \frac{(\rho_p - \rho_g)d^2}{18\mu_g\Theta} \quad (1)$$

where Θ is the drag factor function of the particle Reynolds number, which is the ratio of inertial forces over viscous forces (see Fig. 3 for equation), μ_g is the dynamic gas viscosity, d is the particle diameter, ρ_p is the particle density and ρ_g is the gas density. Given that a turbulent flow can be characterized from the smallest size of eddies (Kolmogorov scale) to the largest scale of eddies (integral length scale), one can evaluate the Stokes number by choosing different flow timescales. Scaling using the Stokes number, the gas-particle slip (velocity difference) and the mass loading (ratio of particle-to-fluid mass in a unit volume) define the gas-particle coupling regime diagram operating in PDCs: ballistic, turbulent suspension (weak coupling with preferential particle concentration, and strong coupling with turbulence induced by the particles forming clusters, with cluster-induced turbulence known as CIT) and granular flow (including bedload transport where particles move mostly along the base of the flow) (Fig. 2).

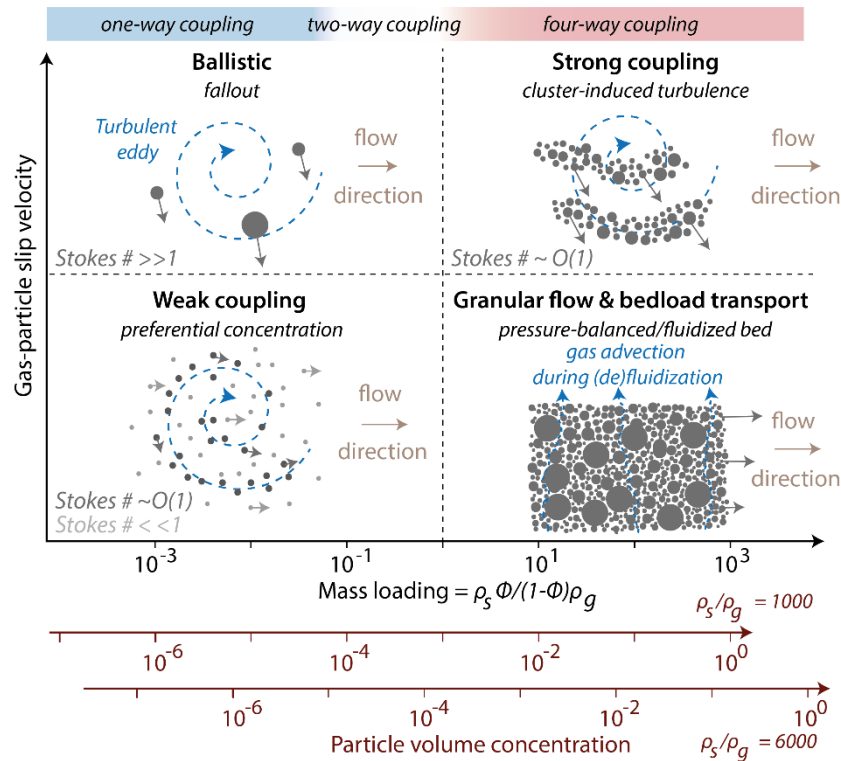


Figure 2. Gas-particle transport regimes in pyroclastic density currents (PDCs) illustrated for two solid-to-fluid density ratio extremes ($\frac{\rho_s}{\rho_g} = 1000$ or 6000 ; lowermost axes) to be expected in PDCs. The various regimes are based on the gas-particle slip velocity and mass loading parameter [F1]. One-way coupling designates particle motion controlled by the fluid drag and pressure gradient; in two-way coupling, particle motion and fluid flow influence each other through momentum feedback; four-way coupling further involves two-way coupling with the addition of particle-particle collisional and frictional interactions (which are two-way). The diverse types of gas-particle coupling control the partitioning of the particles within the flow and ultimately the residence time of the particles within the various layers of the PDCs. In the bottom right regime, we only drew the granular flow regime for clarity, omitting the drawing of the bedload regime.

As stated above, most PDCs are thought to consist of a concentrated layer (basal underflow or bedload), whose behavior is predominantly influenced by particle-particle interactions and possibly hydrodynamic (gas-particle) interactions, and an (upper) more dilute turbulent layer that is density-stratified and where behavior is dominated by gas-particle interactions. Due to the high solid/gas density ratio (~ 1000 – 6000) and the gas phase's buoyancy in PDCs, particle volume concentrations of $> \sim 10^{-4}$ (depending on the density ratio) are needed to sustain a density current. This threshold coincides with the regime where particle-particle collisions (four-way coupling) become significant in the dilute turbulent layer (Fig. 2). This suggests that four-way coupling will

dominate throughout most of the ash-cloud surge layer in PDCs (particularly in very hot PDCs with large solid-gas density ratios).

Predicting the exchanges of mass, momentum and energy between the concentrated and the dilute layers is very challenging and yet essential to understand the evolution of PDC dynamics. Coarse particles settle from the dilute layer and feed the concentrated basal layer while fine particles are elutriated from the underflow. These processes—settling and elutriation—are key mechanisms through which mass, momentum, and energy are transferred between concentrated and dilute layers within a PDC.

2.1c. Key physical processes

In subaerial conditions, ambient air entrainment is most substantial during the initial stages of PDC formation, particularly during column collapse, where rapid mixing begins to dilute and cool the current. As the PDC travels downslope, its relative motion with the ambient air and the substrate generates shear at the flow margins, leading to instabilities. At the outer turbulent edges, shear instabilities, such as Kelvin-Helmholtz (K–H) billows, promote further entrainment of ambient air into the dilute upper layer of the current. This entrainment is most effective at the flow head, lateral margins, and upper regions, depending on the internal density stratification. In contrast, the lower portion of the PDC entrains less air, resulting in limited cooling in that region. A strong density stratification, indicated by a Richardson number (see [Fig. 3](#) for equation) above 0.25, can prevent mixing of cold air into the lower flow region, and thus increase PDC's thermal impact on life and infrastructure. Density stratification could also explain the small variations in thermal data obtained from PDC deposits sampled at various distances from the source. Another shear instability, similar to K-H, occurs at the interface between the flow and substrate during erosion, where the basal layer shears the substrate. These instabilities, observable on scales of

up to 5-10 meters, facilitate the exchange of mass, momentum, and energy between the flow and its surroundings, which impact the flow's runout. Additional instabilities arise at the front of the turbulent, dilute layer and the concentrated basal underflow. In the dilute layer, lobes-and-clefts instabilities form at the leading edge of density currents due to **Rayleigh-Taylor instability**. Lobes and clefts dynamically grow, shrink, merge, or split as coupled features that evolve continuously during flow propagation. In the concentrated layer, friction-driven fingering instabilities may occur at the flow front, where larger clasts migrate to the surface and form fingers that merge to create levées.

Interstitial gas pressure, also called *gas pore pressure*, has a crucial influence on the behavior of the concentrated basal part of PDCs. Pore pressure attenuates the intensity of contacts between solid particles, thus reducing the energy dissipation of the flow (i.e., decreasing the effective friction coefficient), to allow the concentrated basal underflow to behave more like a fluid and travel long distances on gentle slopes, commonly forming flat-topped deposits. Excess pore pressure is the result of drag caused by the relative movement (slip) between settling particles and the upwardly directed interstitial gas flow, which counterbalances the weight of the particles. Pore pressure, P , depends on the relative velocity between particles and gas, U , such that:

$$U = \frac{kP}{\mu_g h} \quad (2)$$

where k and h are the hydraulic permeability and thickness of the granular mixture, and μ_g is the dynamic viscosity of the gas, respectively. According to the Kozeny-Carman equation, which describes fluid flow through a packed bed, the permeability of the bed in the laminar regime depends on three key parameters: the porosity (ϵ) of the packed bed, the mean particle diameter d_p , and the sphericity (ϕ) of the particles. The permeability for a particle Reynolds number (see Fig. 3 for equation) < 1000 is thus defined as:

$$k = \frac{\varepsilon^3 (\Phi d_p)^2}{150(1-\varepsilon)^2} \quad (3)$$

For polydisperse mixtures such as PDCs, the relevant mean particle diameter is the Sauter mean diameter also known as d_{32} , which can be estimated from a weighted particle size distribution as:

$$d_{32} = \frac{1}{\sum_i \frac{x_i}{d_i}} \quad (4)$$

where i marks the bin (sieve), x_i is the mass fraction of each bin (or sieve) and d_i is the geometric mean estimated as $d_i = \sqrt{(d_i \times d_{i+1} + 1)}$.

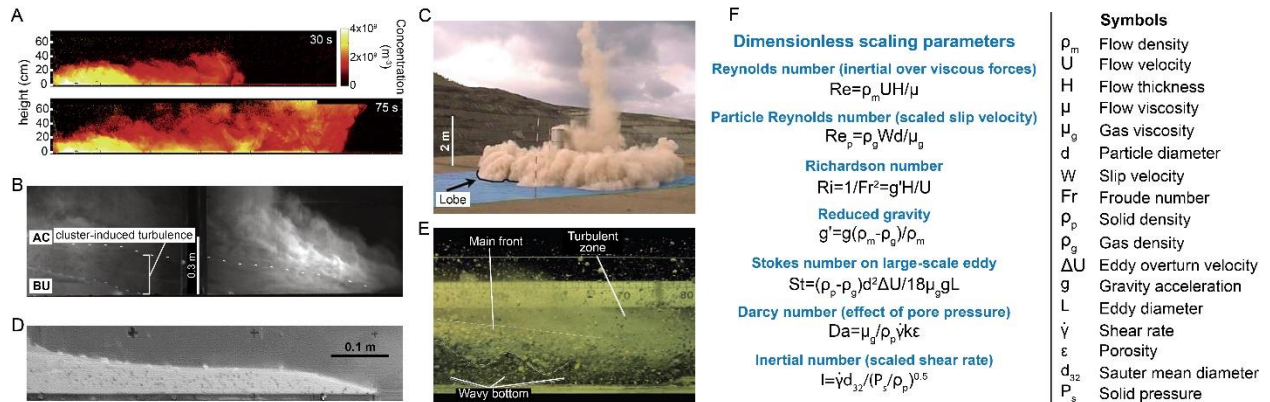
The concentrated layer in PDCs acts as a compressible two-phase flow, wherein changes in particle concentration impart changes in the interstitial pore pressure. Compaction (i.e., increase of flow density) of the mixture will increase pore pressure whereas dilation (i.e., decrease of flow density) of the mixture decreases it, which is known as **pore-pressure feedback** [6]. Excess pore pressure can be generated in the impact zone of eruptive fountains and later during PDC propagation as the granular mixture slows down (i.e., compacts) and the interstitial gas is expelled upwards (i.e., hindered settling) [7]. Pore pressure is enhanced by fragmentation-induced fluidization as the grain size distribution widens due to fragmentation of blocks during transport [8]. Gas released by pyroclasts, burnt vegetation, vaporization of water (ice/snow or surface water, Fig.1F), as well as ingested ambient air that is rapidly heated/expanded at the flow front, also contribute to pore pressure creation. On the other hand, dilation of the granular mixture, for instance when a PDC “jumps” a topographical obstacle (e.g., step, Fig.1G), or accelerates (i.e., Reynolds dilatancy), causes a temporary drop in pore pressure. When the drag due to relative gas-particle movement becomes negligible, the gas pore pressure decreases according to a diffusion law in a characteristic time:

$$t = \frac{h^2}{D} \quad (4)$$

229 where the diffusion coefficient $D = \frac{k}{\varepsilon\mu\beta}$ (5)

230 with β the compressibility of the gas. The progressive decrease in pore pressure and the
231 corresponding increase in granular friction cause the concentrated basal underflow to slow down
232 and stop. The granulometry of PDCs is a key factor in promoting high pore pressure over long
233 periods. As predicted in Eq. 3, non-sphericity of particles, as well as large quantities of fine ash
234 and polydispersity of the pyroclastic mixtures, from primary fragmentation in the conduit or from
235 secondary fragmentation and attrition during transport, confer permeabilities, k , on the order of
236 $\sim 10^{-13} - 10^{-10} \text{ m}^2$ and enable full particle weight support at relative velocities, U , as low as ~ 1
237 mm/s. The runout of the concentrated basal underflow is strongly controlled by the diffusion
238 timescales (cf. permeability and flow thickness), which can last hours in large eruptions with
239 concentrated flows several tens of meters thick. Additionally, material supply from the upper ash-
240 cloud surge can prolong pore pressure diffusion by hindered settling while continuously
241 replenishing the basal underflow.

242



243

244 **Figure 3. A:** Dilute turbulent current of hot talc powder showing air entrainment through surface instabilities.
245 The initial thermal energy of the current and the amount of entrained air control the runout distance [F2]. **B:**
246 A current of polydisperse natural material (e.g., Taupo ignimbrite) is density-stratified and consists of a
247 basal concentrated underflow (BU) and an upper dilute turbulent suspension with mesoscale clusters
248 (cluster-induced turbulence, CIT) (AC) [F3]. **C:** Upper dilute layer of a current formed from vertical collapse
249 of volcanic material ejected initially from a vertical pipe [F4]. **D:** A concentrated flow of fine glass beads with
250 high pore gas pressure propagates like an inviscid fluid [F5]. **E:** The dynamics of a concentrated flow of

volcanic material with negligible pore gas pressure is controlled by particle interactions [F6]. **F:** List of the most relevant dimensionless parameters to scale the processes observed at the laboratory scale.

2.1d. Overspill/detachment processes and mobility

Commonly, small-volume ($< 1 \text{ km}^3$) PDCs are confined within channels due to their gravity driven nature. However, a number of processes trigger the overspilling and detachment of PDCs. Unconfined PDCs can be generated by two main mechanisms: 1) the point of inception is unconfined (e.g., directed blast eruptions); or 2) some or all of the flow mass escapes the channel through overspill or detachment (Fig.1E). Overspill is the process by which the concentrated basal underflow of a channelized PDC, often accompanied by its dilute upper component, flows over the banks of a channel/valley, creating overbank flows and deposits (e.g., [9]). Detachment occurs when the dilute upper layer of a channelized PDC separates from the concentrated basal underflow (e.g., [9]). PDC overspill and detachment, individually and in combination, have been responsible for some of the deadliest PDC-related volcanic disasters in recorded history due to their ability to inundate and destroy areas seemingly distant from typical PDC pathways (up to nearly a kilometer from the channel). The causes of such processes are typically related to the combination of changes in syn-eruptive topography and in flow characteristics (mass flux, volume, or velocity).

Overspill and detachment can be caused both by changes to topography as well as the changes to the characteristics of the PDCs themselves during an eruption. Constriction of the width and/or depth of a channel can reduce its cross-sectional area (and therefore volumetric capacity), causing vertical and/or lateral expansion of the PDC, thereby promoting overspill and detachment (e.g., channel width constriction: Merapi 1994, 2006; channel depth constriction: Merapi 2010, Fuego 2018). This change in channel morphology can be natural (e.g., progressive infilling of the channel by previous PDCs, lahars, or other sedimentary depositional processes) or human-made (e.g., caused by erosion or built structures like sabo dams). Pulsatory behavior during an eruption

can also increase the likelihood of overspill and detachment as rapidly fluctuating succession of PDC pulses infills a channel, dramatically reducing its capacity and promoting overspills of the later pulses. High channel sinuosity and sharp break in slopes promote PDC overspill and/or detachment, where the associated overbank flows and surges spread laterally downstream due to preservation of momentum (e.g., Soufrière Hills 1997, Merapi 2010, Fuego 2018). Sudden breaks in slope also promote detachment of the PDC's upper dilute layer (e.g., Ngauruhoe 1975). Finally, variations in internal properties (e.g., mass flux and momentum) of successive PDC pulses during a single eruption can also increase the likelihood of overspill and detachment. See [section 4.1](#) and [case study 1](#) for details.

Case study 1: The June 3rd, 2018, PDC events at Fuego volcano (Guatemala)

The June 3rd, 2018, eruption of Fuego volcano (Guatemala) was an unusually large paroxysmal eruption for this volcano, and its impact on exposed populations and infrastructures was the largest since eruptions in 1932 and 1974 (see [\[E4\]](#) for details). On June 3rd, 2018, a complex sequence of PDCs inundated all sectors around the volcano. The largest volume PDCs propagated >12 km on the southeastern flank with PDCs depositing ~50 million m³ of pyroclastic material. The large volume and far-travelled PDCs killed several hundred people both along the RN-14 road and in the village of San Miguel de Los Lotes (SMLL). The two main causes for the high death toll during this eruption were: 1) the generation of large, voluminous PDCs with high mass-fluxes from continuous headwall failures and rapid retrogressive collapses of a thick and large portion of the oversteepened volcanoclastic material that was accumulated in the old collapse structure of the SE flank; and 2) the rapid (~10 min.) infilling of a distal channel section by PDCs in the early afternoon that crossed the RN-14 road and led to major overspills, where both a channel constriction and 90° bend allowed the subsequent PDC pulses to advance in the direction of SMLL (e.g., [\[10\]](#)). The PDC generation by partial collapse of recently accumulated material at and around the summit provided the readily available large volume of material required to produce the long runout flows that inundated SMLL. In particular, the progressive infilling and then subsequent overspills allowed for overbank flows to be directed toward the community of Los Lotes. This eruption has illustrated once again that the behavior of PDCs remains difficult to predict, demonstrating the need for an improved understanding of their internal dynamics and hazard assessment.

2.2. PDC deposits

2.2a. Types of PDC deposits

PDC deposits encompass a wide spectrum of **lithofacies**, reflecting a range of eruptive styles and generation mechanisms, magma physicochemical properties, and external factors (e.g., topography, external water) that determine the final sedimentological features of each PDC deposit. PDC deposits are typically dominated by juvenile material (i.e., magma emitted during the eruption), along with crystals and accidental lithics (clasts entrained from the conduit or ground surface), except in cases of oversteepened volcanoclastic collapse, where lithics can become the dominant component [10]. Historically, the classification of PDC deposits was approached using terminology based mainly on the generation mechanism and/or the inferred transport mechanism. However, there is now recognition that flow stratification and flow deposit type can be variable for a given flow along its path. Here, we discuss examples of key PDC deposit types, including ignimbrites, block-and-ash flow deposits, and pyroclastic surge deposits. All flow types listed in Table 1 that do not involve ice can generally be classified into one of these three categories.

The term ignimbrite is commonly used to describe deposits that result from the partial or total collapse of explosive eruption columns or fountains, including during caldera-forming eruptions, irrespective of the parent magma composition [2]. However, the lithofacies associated with ignimbrites can also be found in PDC deposits formed by lateral/hydrothermal blasts, block-and-ash flows, scoria flows, pyroclastic surges and base surges.

Following [2], ignimbrites consist predominantly of massive, poorly sorted (sometimes welded) juvenile and lithic ash, blocks, bombs, pumice or scoria. However, different degrees of stratification and/or grading, and changes in spatial lithofacies are also a common feature of these deposits. In the largest caldera-forming eruptions, ignimbrite deposits have volumes greater than 1,000 km³ and indicate PDC runouts of a few to >300 kilometers. Key flow and deposit

parameters, such as the runout, volume and area can be used to evaluate the magnitude and intensity of the PDC-forming eruptions (e.g., [2, 11, 12]).

Block-and-ash flow deposits are generally valley-controlled and found on overbanks when overspill occurs. These deposits are associated with concentrated PDCs generated by the gravitational collapse of lava domes, lava flows or proximal tephra. They are poorly sorted massive to graded deposits, consisting of relatively dense lava/dome blocks and boulders embedded in an ash matrix.

Pyroclastic surge deposits veneer topography and are made of massive to stratified/laminated deposits formed by the deposition of relatively fine pyroclasts (< a few cm) from a turbulent flow. The development of significant lateral lithofacies variations, as well as the occurrence of ash aggregates and plastic deformation structures related to interaction with external water, are also common features. All blast-related deposits, including lateral and hydrothermal blasts, are considered types of pyroclastic surges and often display diagnostic features such as a tripartite internal architecture [13].

Classifying PDC deposits according to their physical characteristics has the advantage of facilitating comparison of eruptions and deposits from around the world, enabling a global understanding of PDC processes. However, labeling deposits can be problematic, especially when applied to large and internally complex deposits associated with PDCs that have undergone drastic changes in flow dynamics over space and time.

2.2b. Links between deposit facies and internal flow structure

While analysis of deposit characteristics such as geometry and runout can provide key information regarding, e.g., the mass flow rate of a PDC, interpretation of the lithofacies at a given outcrop is not straightforward. One of the main purposes of a detailed description of lithofacies in a PDC

deposit is to distinguish the number of flow units within it. However, such studies should always consider that an outcrop represents an incomplete view of a current at that location. PDC deposits must be considered (from bottom to top) as a succession of snapshots of different depositional regimes over time. From this perspective, each lithofacies is related to a different point in the temporal and spatial evolution of a PDC, which helps identify quasi-stable and unstable phases (e.g., waxing and waning at the front) of a current. The spatial and temporal variability, which characterizes the sedimentation parameters and regimes of PDCs, makes comparisons between lithofacies of a single PDC at different locations more difficult.

The physical characteristics of a PDC deposit at a given outcrop can be used to infer the conditions within the lower flow boundary zone (LFBZ, [Fig. 4A](#)) [3], which is the region connecting the deposit to the current. While its definition is debated, the LFBZ can be characterized as the zone where significant changes in rheological flow properties occur (i.e., velocity gradients and, for dilute PDCs, concurrent variations in particle volume concentration). The base of the LFBZ corresponds to the static surface of the substrate/deposit, while its center is inferred to be located at the lower flow-substrate/deposit boundary. This inferred boundary is defined by the height where the exponential velocity profile transitions into a linear, Bagnold, or logarithmic profile, depending on the rheology.

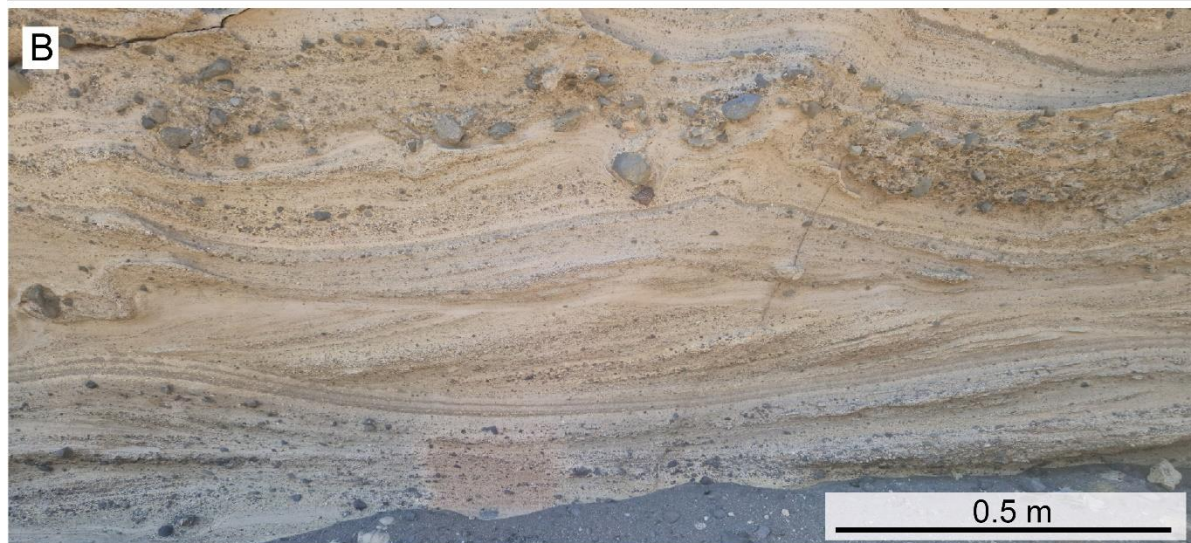
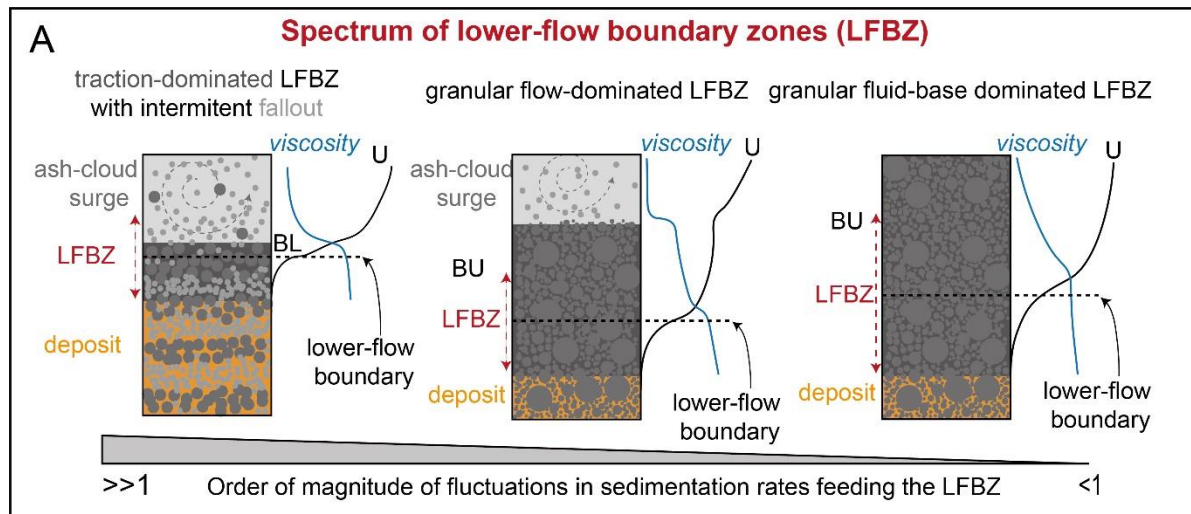


Figure 4: A: A sketch of the spectrum of lower-flow boundary zones (LFBZ) in pyroclastic density currents (PDCs), defined by rapid vertical mixture viscosity changes, which are strongly influenced by vertical gradients in particle volume concentration and shear rate (base of LFBZ: static substrate/deposit boundary; center of the LFBZ: aligns with the lower-flow boundary defined as the height where the exponential velocity profile (starting at the static boundary) shifts into a different form such as logarithmic, linear or Bagnold-like). Note the schematic viscosity profiles are illustrated on a log-scale whereas the schematic velocity profile (U) is on a linear scale. Fluctuations mentioned are dimensionless (standard deviation/average). BU: basal concentrated underflow layer. BL: bedload layer, as in Fig.1. **B:** Dilute PDC deposits emplaced by traction-dominated LFBZ at the Montaña Pelada tuff ring (Tenerife). **C:** Deposit from dilute PDC with concentrated underflow emplaced by granular flow-dominated LFBZ and granular-fluid based LFBZ from the 1883 Krakatau eruption (Indonesia) to the NW of Sertung island.

Case study 2: The May 18th, 1980, PDC events at Mount St. Helens (USA)

The afternoon of the 18 May 1980 eruption of Mount St. Helens (Washington, USA) was dominated by numerous column-collapse and boil-over PDCs. These PDCs deposited across a wide range of terrains, including the steep (30°) flanks, relatively smooth terrain along the eastern pumice plain (5°), and hummocky terrain along the western side of the pumice plain (5-15°). Deposits within the pumice plain are predominantly massive and poorly sorted, indicating deposition from the base of concentrated, partially fluidized PDCs [14]. Despite the massive nature of the deposits, portions of the deposit exhibit particle fabric aligning with flow directions, self-channelization, and blocks entrained from debris avalanche hummocks, which indicate shear and erosion were important during the depositional stages inside the LFBZ of the currents. Additionally, flame structures inside the deposits indicate elevated pore fluid pressures just after deposition that enabled mixing at the flow-bed interface [15].

In contrast, deposits along the steep flanks are cross-stratified and comprised of compound bedforms with waveforms up to 40 m in length. Evidence for erosion, including entrainment of substrate clasts and bedform truncations, is pervasive. Bedforms transition to massive deposits as the slope lessens, becoming predominantly massive in the eastern pumice plain. The gradual, downslope transition from cross-stratified to massive deposits indicates a thickening of the LFBZ due to suspension sedimentation from the overriding current. The transition into massive deposit on shallow slopes suggests that the LFBZ transitioned from traction-dominated to granular-flow dominated (see Fig. 4) depositional regimes. Such variations indicate that slope has a significant influence on PDC dynamics, with the lateral grading of deposit characteristics revealing the morphodynamic nature of PDCs. This series of observations, combined with experimental and numerical simulations described in [14], highlights the complex nature of PDCs, as well as our ability to infer some internal flow dynamics from deposit characteristics.

The deposit facies, architecture, and particle size distribution are used to infer LFBZ conditions, particle concentration during transport, and depositional/transport regime. Small and medium-scale PDCs ($< \sim 1 \text{ km}^3$) typically form deposits that can be unequivocally interpreted (from the deposit facies, architecture, and grain size distribution) as dominantly concentrated or dilute PDCs. Such PDCs are fed over short durations, resulting in small volumes and relatively thin deposits. As a consequence, even when a concentrated basal underflow is present, it defluidizes in a few minutes, and exhibits limited runout. Therefore, PDC density stratification then becomes one of the endmembers shown in [Fig. 1](#). However, in large-scale PDCs ($> 1 \text{ km}^3$), processes within the LFBZ can become disconnected from the parent flow because clasts are transported first by a turbulent dilute flow and then within a fluidized concentrated basal layer. For instance, a thick dilute and turbulent PDC (in a depth-averaged sense) (e.g., 1 km thick) can develop a concentration gradient where concentration near the base is high ($> 1 \text{ vol.}\%$), enabling rapid sedimentation (due to strong coupling with mesoscale clusters and high particle volume concentration) to occur over a long duration and distance. If the basal underflow becomes a fluidized thick basal layer, it can acquire its own momentum and behave independently from the parent turbulent PDC. Examples of such flow dynamics may include the CE 1883 Krakatau ([Fig. 4C](#)), 38.8 ka Campanian or AD 232 Taupo ignimbrites. This independence prevents the use of the deposit characteristics at the outcrop scale to provide information on the current as a whole, necessitating analyses of large-scale trends instead.

Erosional contacts and bedding within a PDC deposit reflect the fluctuating conditions (e.g., velocity, concentration) within a LFBZ with stepwise aggradation, which is attributed to changes in the mass flux at the source and/or changes in density stratification that occurred during propagation of the current (e.g., turbulent fluctuations, interaction with topography). Individual beds may be in the order of millimeters to meters in thickness. The presence of multiple beds may represent the passing and deposition of multiple distinct currents but can also be related to the

passing of multiple pulses or, at a particle scale, turbulent eddies, past a given location. Analysis of bedforms through measurement of their wavelength, particularly for deposits from dilute PDCs (Fig. 4B), can be used to calculate the local dynamic pressure, a key parameter describing the potential impact of PDCs [E4].

Grain size is a key measurement when identifying, analyzing and interpreting PDC deposits. The grain size of a deposit is controlled by the initial grain size in the current, and the current characteristics at each location. Due to the turbulent nature of the parent current, deposits from dilute PDCs become finer grained and better sorted with distance (commonly lapilli-to ash-rich). In comparison, clasts within deposits from concentrated PDCs, including pumice flows and block-and-ash flows, can range from several meters in length to sub-micron-sized particles. This range in grain size provides a unique challenge in terms of measuring the total deposit grain size distribution at both the outcrop and the whole deposit scale.

PDC deposit grain size information, typically presented in Phi units ($\phi = -\log_2 D$), where D is the grain size in millimeters, can be displayed in several ways. The most common is as histograms of grain size distribution by half phi or full phi size bins (Fig. 5), which enable identification of different distribution modes. Commonly, PDC deposits from concentrated currents, like block-and-ash flows, are multimodal, while individual layers within surge deposits commonly have a single mode (Fig. 5A) due to their dominant turbulent transport mechanism. Several statistical parameters are used to describe and compare grain size distributions between deposit types and locations, and/or different eruptions and volcanoes; including the median (Md) grain size, which measures size at the 50th percentile, and sorting coefficient, which measures the spread in grain size. Longitudinal changes of Md and sorting (Figs. 5B and 5C, respectively) within a single PDC unit can help decipher the dominant transport mechanism. Fig. 5D shows that fields for different deposit types largely overlap, so trends are often more useful than absolute

position when plotting Md against sorting coefficient data. The “dilute PDC” and “concentrated PDC” fields reflect the dominant dilute and concentrated transport mechanisms, respectively.

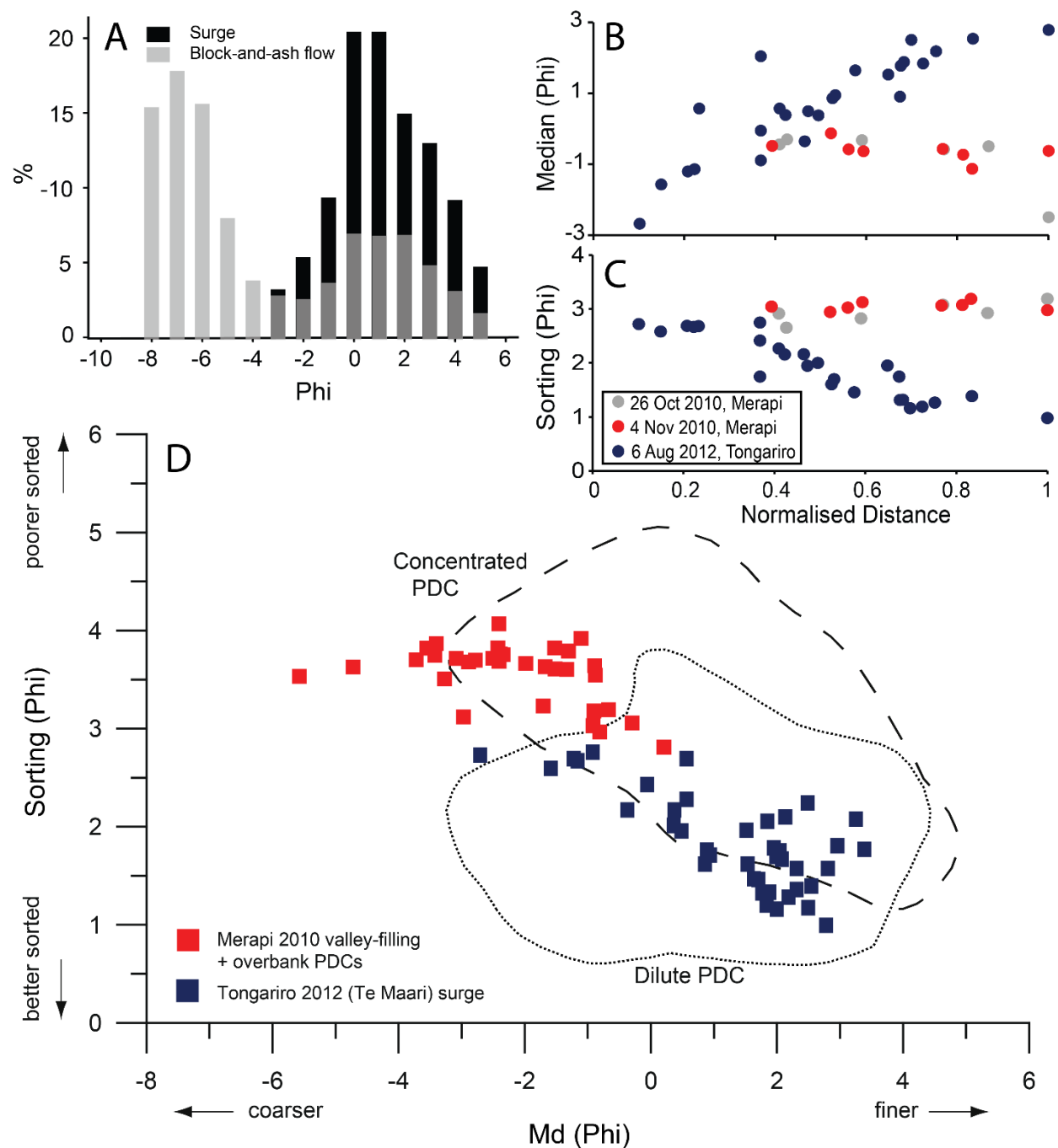


Figure 5: A: Example grain size distributions from a bimodal block-and-ash flow (KG2-OB2) and unimodal surge deposit from the 2006 eruption of Merapi showing key differences in distributions sometimes seen

419 for these deposits [F7]. The shading of the fine mode of block-and-ash flow is used to see the data where
420 it overlaps with the surge data. **B:** Median grain size and **C:** sorting coefficient with distance from source
421 for block-and-ash flow deposits produced during the 2010 eruption of Merapi [F8] and surge deposits (Unit
422 A) from the 2012 Te Maari eruption of Mt. Tongariro [F9]. **D:** Walker diagram showing Dense flow (dashed
423 line) and surge (dotted line) fields, overlain by grain size data from the Merapi 2010 block-and-ash flow
424 deposits [F8] and 2012 Te Maari surge deposits [F9] highlighting the differences in characteristics between
425 different flow types. Pyroclastic density current = (PDC).

Deposit grain size, particle shape, and texture all provide information on the primary fragmentation (magmatic or magma-water fragmentation), secondary fragmentation mechanism, and particle transport. Particle rounding and fine ash generation occur due to abrasion, with the degree of roundness dependent on the duration of abrasion and the type of particle.

Importantly, post-depositional welding, alteration, and erosion may affect interpretations of flow conditions. Welding can make it difficult to identify individual particles, while alteration may lead to a change in color of a deposit and weakening of particles, preventing the identification of original textures. In contrast, the degree of pre- or syn-eruptive hydrothermal alteration and oxidation of PDC deposits can also help correlate different PDC units from various stratigraphic sections.

3. Review of methods to characterize PDCs and their deposits

3.1. Inferring flow properties from field measurements and deposit characteristics

Field-based data have not only shaped the historical evolution of PDC conceptual models but continue to play a key role in benchmarking physical models, analogue experiments, and numerical simulations. The unpredictable and hazardous nature of PDCs make real-time direct or geophysical observation challenging. Thus, quantitative field-based approaches to estimate flow properties from PDC deposits have become an invaluable source of information.

Grain-size distribution is a key metric, as it provides insight into the dominant transport mechanisms within the flow, such as whether sediment was carried primarily by granular interactions or turbulent suspension. For dilute PDC deposits and the matrix of concentrated deposits, samples are typically collected and sieved to quantify the proportions of different size fractions. Larger clasts (>0.1 m) are often measured separately in situ, and photogrammetry techniques are increasingly used to map their distribution and dimensions. In dilute PDC scenarios, turbulent boundary layer theory enables the estimation of dynamic pressure profiles

using sedimentological data from stratified deposits such as layer thickness [16], grain-size distribution, particle size, shape, and density. For concentrated PDCs, lithic blocks derived from the underlying substrate can be used to estimate the velocity of the parent flows using a few approaches. One method is to focus on estimating the minimum aerodynamic drag force to entrain/carry large lithic boulders. Another method is based on the concept that large substrate-derived clasts are entrained in PDCs by an upward force related to the vertical pore-pressure gradient generated at the sliding head of granular flows. In both strategies, the main input data include the shape, size, and density of the lithic clasts, along with certain assumptions such as PDC bulk density and the initial position of the clasts before being entrained. Furthermore, flow properties in concentrated PDCs can be estimated using additional sedimentological features such as flame structures. Recumbent flame structures, exclusively found in concentrated flows, originate from granular shear instabilities at the flow-bed interface. Flame structures can be used to calculate the minimum basal slip velocities and deposition rates at the time of instability initiation from their wavelength [15].

Direct and indirect temperature measurements suggest that PDCs have a broad spectrum of thermal states, which cannot always be interpreted directly from the lithofacies of the related deposits, except for the case of welding in ignimbrites. Therefore, quantitative estimation of the temperature of PDCs is commonly derived by charcoal reflectance and paleomagnetic methods. The common presence of charred wood fragments in PDC deposits makes charcoal reflectance a powerful and accessible proxy to estimate PDC temperatures. Progressive thermal demagnetization of accidental lithic clasts incorporated into PDCs is another widely used method to estimate emplacement temperatures and distinguish between primary PDC deposits and secondary deposits affected by reworking. In recent eruptions, PDC temperature has been interpreted from charred wood, melted plastic containers and clothing, and thermal damage to infrastructures. Another useful method to obtain flow dynamic information from the magnetic

properties of PDC deposits is the anisotropy of magnetic susceptibility, which is mainly used to define flow directions and identify the source of PDCs. Please see [E4] for various applications using these methods.

Please add QR1 code for 'Further reading: Flow properties from deposit characteristics' here

3.2. Analogue experiments

Analogue PDC experiments, at reduced length scales but in controlled environments, aim to investigate fundamental mechanisms of PDCs. Results of experiments assist in interpreting natural deposits and serve to define the physics on which PDC models and their numerical simulations are based. Length scales of analogue experiments have typically been 1 meter to 10s of meters. Experiments are carried out with either analogue or natural granular materials, depending on the objective. Each configuration has its pros and cons. Small-scale experiments can be repeated many times for statistical treatment of results but often present limitations in terms of scaling. For example, the degree of turbulence (assessed using the Reynolds number, Re) in experiments (typically $Re < 10^4$) is much lower than in natural flows (Re up to 10^9). Large-scale experiments, on the other hand, are difficult to repeat because of the large quantities of material involved, but they provide access to a wider range of physical regimes (e.g., wide range of Stokes number, higher Reynolds numbers up to $\sim 10^5$) and metrology instruments are often easier to implement and not as disruptive when placed in-situ. Analogue well-characterized granular materials are chosen when experimentalists seek to investigate, for instance, the specific effect of particle size or density on flow dynamics. Natural pyroclastic materials are selected to address the complexity of natural phenomena due to the wide ranges of particle size, density, and shape. Experiments with gas-particle mixtures released onto an inclined or horizontal plane provide various insights into the transport and deposition mechanisms of particles (Fig. 3). Scaling is fundamental to estimate the degree of dynamic similarity between experiments and PDCs. This

is achieved by comparing dimensionless numbers that are generally ratios of forces (or stresses) or timescales and whose values characterize physical regimes. The most frequently used dimensionless numbers are given in Fig. 3, and their use ensures that experiments are relevant to processes occurring within PDCs. A notable common feature of experiments is that the concentrated basal part of PDCs consists of a head that slides (i.e., basal slip) over the substrate and precedes a body where the deposit forms by progressive or stepwise aggradation (see references in caption of Fig. 3).

Please add QR2 code for 'Further reading: Analog experiments' here

3.3. Numerical modeling approaches

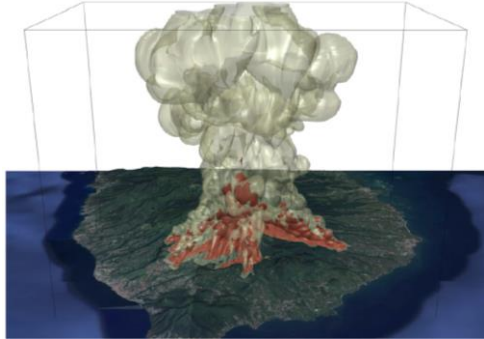
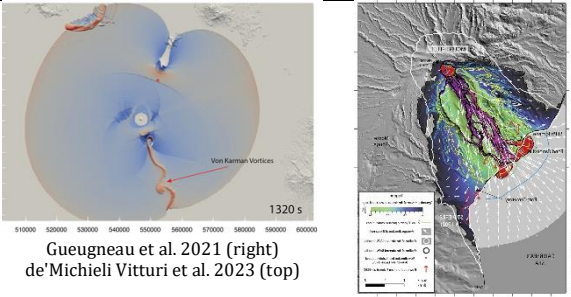

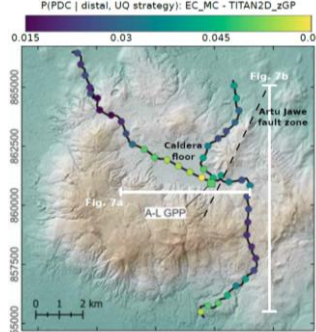
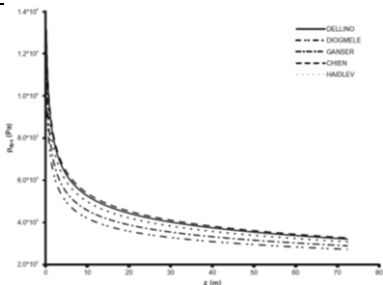
PDCs are some of the most complex particle-laden multiphase flows on Earth, so modeling their behavior numerically is especially challenging and requires simplification of physical processes. Results from numerical models depend strongly on the selection of input parameters and on the assumptions built into the models, as summarized in Table 2. The simplest approaches are one-dimensional (1D) and kinetic, or zero-dimensional (0D), models. These models are orders of magnitude faster to run than more complex models and can provide rapid assessments of PDC hazards, often within a few minutes. However, this efficiency comes at the cost of simplified physics and limited detail in flow representation. Two-dimensional (2D) models solve the shallow-water equations by averaging flow properties along the vertical axis. They have been widely used to investigate the dynamics of past PDCs and to develop probabilistic hazard maps. Their relatively short computational times, often under 24 hours on a desktop computer, make them practical for many applications. More recently, two-layer depth-averaged models have been developed to simulate interactions between dilute and concentrated layers, which represents a significant advancement in capturing internal flow structure. Three-dimensional (3D) two-phase flow models are the most complex. These solve the full Navier-Stokes equations for mass,

momentum, and energy. They are capable of representing both dilute and concentrated regimes within a PDC, including interactions between layers and between the current and natural topography. Although computationally intensive, often requiring days to weeks on a supercomputer, 3D models provide the most detailed representation of PDC behavior. They have been used to reproduce natural events and are increasingly applied alongside small- and large-scale experiments to benchmark model performance and explore flow properties that are difficult to measure directly, such as internal 3D velocity fields.

Aside from 0-3D numerical models, other numerical solvers invert the flow properties, mainly based on the turbulent boundary layer approach, from field deposit datasets and the damage they impart on vegetation. Finally, many PDC models can be used in conjunction with statistical models to build robust probabilistic hazard assessments. For example, this combined approach can be used to calculate the probability of inundation at any given location or area around a volcano. While Monte Carlo methods are easy to implement and can practically explore any range of scenarios, they can become prohibitively computationally expensive due to the large number of simulations required to properly propagate the uncertainty from model input parameters (e.g., volume, source location, rheology, etc.) into model outputs (e.g., spatial PDC inundation). With statistical emulators (e.g., Gaussian Process emulators), a smaller set of simulations is used to build a reliable substitute, or surrogate model, of the PDC model. Thus, the emulator can provide estimates of output values (e.g., flow thickness, velocity, etc.) for any value of the model parameters (tried or untried). This enables both uncertainty quantification at tractable computational costs and probabilistic hazard assessment using complex simulators. However, all models suffer from fundamental and sometimes computational limitations, and their respective use depends on the aim of the study. In the future, the integration of more robust field-based and laboratory datasets, in combination with leveraging GPU-based modelling, will likely reduce such limitations and make probabilistic PDC modelling more efficient for hazard purposes.

547 **Please add QR3 code for 'Further reading: Modeling of Pyroclastic Density Currents' here**

548 **Table 2: Examples of 3D to 0D model types, together with their strengths and weaknesses.**

Type of Model and name	Example	Strength	Limitations
3D (MFIx, OpenPDAC, PDAC)		Capture spatial and temporal polydisperse gas-particle four-way coupling and interactions with complex geometry (topography). Can be used along experiments to explore granular/fluid mechanics of complex multiphase systems.	Require subgrid models for closure terms (drag, stress tensor, subgrid turbulence, effective fluid viscosity) Too expensive to explore epistemic uncertainty on multiple parameters
2D (IMEX_Sflow2D, Titan2D, VolcFlow, SHALTOP, two-layer by Shimizu et al. 2019)	 Gueugneau et al. 2021 (right) de'Michieli Vitturi et al. 2023 (top)	Relatively fast and use 3D topography. Can be used to explore epistemic uncertainty. Can be made of two-layers: dense and concentrated.	Is limited by our understanding of granular flow rheology (concentrated regime). Does not account for 4-way coupling (settling) and some models do not include entrainment of ambient fluid, for the dilute regime. Inherent limitations with the depth-average approach
0D (kinetic model such as energy line/cone) 1D (box model, Bursik and Woods, 1996)	 (c) Combined inundation map	Fast and can be used to explore a wide range of input parameters and capture some of the effect of topography	0D: Highly simplified physics 1D: captures the key physics, settling and entrainment but not necessarily the effect of topography
Statistical (zero Gaussian Emulator, zPG)	 Tierz et al. 2024	Gaussian Emulator: can be applied to any model. It can assess new distributions of input parameters almost instantaneously.	The emulator mirrors the limitations of the numerical model is based on and has issues dealing with discontinuities (zero problem or very sharp changes in thickness despite very small changes in input parameters).
Flow properties from deposit characteristics or damages (Clarke et al. 2000, Burgisser et al. 2002, PYFLOW_2.0)	 Dioguardi et al. 2017	Allows quantitative inversion of the deposit grain-size distributions (GSDs).	Neglects 4-way coupling on the drag laws. Estimates only a instantaneous dynamic pressure and not the fluctuations. Limited to a deposit sequence from dilute pyroclastic density current (PDC)

549

550 **3.4. Geophysical data**

551 Scientists apply a variety of geophysical techniques, ranging from satellite observations to
552 ground-based measurements, to collect data about PDCs and their deposits ([Table 3](#)). The types
553 of data collected using geophysical methods are often unavailable or unobtainable using other
554 methods. These data range from real-time measurements obtained from monitoring networks
555 during eruptions to geophysical assessments of PDC deposits after eruption. Example
556 applications of seismic, infrasound and radar monitoring networks include: 1) the use of seismic
557 monitoring networks in tandem with camera networks to identify eruption pulses; 2) the use of
558 infrasound (the detection of acoustic signals) to rapidly detect eruptive activity in real time,
559 sometimes from great distances, including PDC-related activity; and 3) the use of radar
560 techniques for estimation of PDC velocity, direction, volume, and runout (see [Table 3](#) for
561 examples). These methods can be particularly helpful for tracking PDC activity at night or in poor
562 visibility. Radar techniques have been also used to reconstruct the velocity profiles of eruption
563 plumes and PDCs (and their particles) in real time, providing important data for understanding
564 and modelling internal flow dynamics. Geophysical satellite techniques have become particularly
565 useful tools for identifying and mapping PDC deposits after eruptions, especially in scenarios
566 where extensive field investigation is not possible. Comparison of different types of satellite-
567 obtained data (e.g., SAR, lidar, and TanDEM-X) are frequently used to create high quality pre-
568 and post-eruption digital elevation models (DEMs) and digital surface models (DSMs), which can
569 be used to delineate PDC deposits and to determine their thickness, area, and volume (see [Table](#)
570 [3](#) for examples). Ground-penetrating radar and 3D seismic data are also sometimes used to
571 investigate the stratigraphy and distribution of PDC deposits, particularly in difficult-to-access
572 locations, including submarine environments.

Please add QR4 code for 'Further reading: Geophysical data' here

Table 3: Geophysical methods used to study pyroclastic density currents (PDCs). DEM=digital elevation model; DSM=digital surface model; SAR=synthetic aperture radar.

Method	Variants	Purpose	PDC Applications and Examples
Monitoring networks	<ul style="list-style-type: none"> Seismic Radar Infrasound 	<ul style="list-style-type: none"> Detect (non-visible) signals from eruptions in real time Estimate velocity of various eruption components 	<ul style="list-style-type: none"> Identify eruption pulses to recreate PDC sequences Remotely identify eruptive events (including PDCs) in real time Estimate PDC velocity, direction, volume, and runout Track PDC activity at night or in poor visibility Identify collapsing eruption plumes which may lead to PDCs Analyze particle velocities within PDCs to understand internal dynamics
Satellite techniques	<ul style="list-style-type: none"> SAR Lidar TanDEM-X 	Create high quality pre- and post-eruptive DEM and DSM data	<ul style="list-style-type: none"> Delineate PDC deposits and determine their thickness, area, and volume Map PDCs in post-eruptive scenarios where extensive fieldwork is not possible
Subsurface/submarine techniques	<ul style="list-style-type: none"> Ground penetrating radar 3D seismic data 	Create seismic reflection data related to travel time through PDC deposits	Reconstruct stratigraphy and distribution of deposits in hard-to-reach locations, such as underwater

4. Recent advances

4.1. Control of eruption discharge rate on PDC runout distance

A relationship between mass discharge rate (Q) and PDC runout (R) has long been known to exist for dilute PDCs (e.g., [11]). A new compilation of data from a statistically significant number of eruptions (>50), with R and Q varying over two and five orders of magnitude respectively, shows two distinct power law relationships $R_d = \alpha Q^n$ and $R_c = \alpha' Q^{n'}$ for dilute or concentrated PDCs, respectively, with constants α and α' [12]. For dilute PDCs, whose propagation is largely unaffected by topography, the exponent $n=0.47$ is very close to the theoretical value of 0.5 determined for currents propagating radially and with particle settling. In contrast for concentrated PDCs, whose mass decreases progressively through particle settling, the exponent $n'=0.36$ is smaller than the value for dilute currents. This may be explained by the fact that PDCs from smaller eruptions (less than 1 km^3) often travel farther due to valley channeling, while larger-volume PDCs spread more radially, which reduces the slope of the power-law relationship. These power law relationships can be used to deduce discharge rates from observed runouts or, conversely, to predict runouts from possible discharge rates in the context of hazard assessments. For example, within a 95% prediction interval, knowing the runout gives a wide range of possible discharge rates that can vary by more than a factor of 10. In contrast, if the discharge rate is known, the corresponding runout typically varies by a factor of about 3. The range in runout distances is not negligible and may be due to parameters such as particle polydispersity and related particle settling velocities, temperature of dilute PDCs, and non-negligible effects of topography, in particular for concentrated PDCs.

4.2. Benchmarking of PDC hazard models

Numerical models of PDCs are widely used for fundamental research and for hazard and risk modeling that supports decision-making and crisis management. Recent advances have allowed the development of a consensual validation and benchmarking procedure to assess the performance of numerical models used for PDC hazard assessment [17]. This framework

provides critical information about the uncertainties in hazard assessments that depend on these models. The methodology is based on a hierarchical process of comparing computational solutions with experimental datasets at different levels of complexity, from unit problems (well-known, simple computational fluid dynamic problems), through benchmark cases (complex setups having well constrained initial and boundary conditions) and subsystems (decoupled processes at the full scale), up to the fully coupled natural system. Among validation tests, this framework also further distinguishes between confirmation (comparison of model results with a single, well-constrained dataset) and benchmarking (inter-comparison among different models of complex experimental cases). The latter is of particular interest for PDCs, where different modeling approaches and approximations can be adopted to deal with the large epistemic uncertainty of the natural system. A series of community-wide initiatives have been carried out during the last ten years, in conjunction with the design of new large-scale laboratory systems where experiments are able to synthesize a wide range of fluidized granular currents under simplified initial and boundary conditions, like the PELE (i.e., [18]) and PyroCLAST [19] apparatus. Results of these collaborative efforts provide critical datasets that can be integrated into global databases of volcanic mass flows (e.g., FlowDat) for a coherent inter-comparison of numerical model results.

4.3. Advances in understanding of less commonly considered PDC hazard processes

Beyond the aforementioned PDC generation mechanisms (see [section 2.1a](#)), there are many other generation scenarios that have been observed in historical PDC-forming eruptions but are hard to identify in the geological record. These uncommon mechanisms for generating PDCs are inherently hazardous due to their rare occurrence and lack of consistent precursors; they are consequently often overlooked in hazard and risk mitigation plans. For instance, unexpected secondary inland-directed PDCs can be produced by the explosive interaction of primary PDCs

and water bodies (e.g., Soufrière Hills volcano). In recent years, it has been increasingly recognized that the remobilization of loose, sometimes hot, pyroclastic material on steep slopes of the volcano also poses a significant hazard. This material can be remobilized by subsequent PDCs or gravitational collapses, producing secondary PDCs with unexpectedly large volumes and mobilities (e.g., Fuego 2018). Moreover, PDCs generated by rapid lava spill outs, sometimes during crater wall collapses, have been recorded at several volcanoes (e.g., Arenal volcano). During these events, PDCs are generated during low-explosivity eruptions (spattering/strombolian) or during inter-eruptive periods. PDCs can also be generated during effusive eruptions through the explosive interaction of lava flows with ice, snow or water-saturated sediments (e.g., Klyuchevskoy volcano). Finally, phreatic eruptions, which are themselves difficult to forecast, can generate PDCs (e.g., Whakaari volcano).

Please add QR5 code for 'Further reading: Less commonly considered PDC hazard processes' here

4.4. Role of PDCs in cascading hazardous events

Several indirect hazardous processes can also be related to PDCs, including fires or secondary phreatic explosions triggered by burial of water streams under PDC deposits. PDCs also deliver a large amount of loose material that can be remobilized by wind (ash-resuspension) and lahars over long distances and over tens of years. However, one of the most significant indirect hazards related to PDCs is their ability to trigger tsunamis upon entering water bodies. The concentrated basal underflow plays the dominant significant role in wave generation, while the dilute upper part of the current can travel above water for tens of kilometers. A key example of this PDC tsunami generation occurred during the 1883 eruption of Krakatau in Indonesia. In the last few years, a large effort has been made to better understand PDC-related tsunamis through numerical modeling and analogue experiments. In these studies, wave features have been found to be

related mainly to the volume, mass flux and grain size distribution of the PDC rather than other parameters such as bulk density. Furthermore, ash-rich character and high gas pore pressures of concentrated basal underflows increase the potential for PDCs to generate tsunamis since they prevent energy dissipation by seawater percolation into the flow.

Summary

Pyroclastic density currents (PDCs) are deadly flows of ash, gas and rocks that form during volcanic eruptions and remain one of the greatest volcanic hazards. Understanding how these currents form and what affects their dynamic flow behavior in time and space is fundamental to improving our forecast models that support hazard assessments. Despite significant advances in our understanding of PDCs from field, remote sensing, and theoretical and experimental studies, there are still fundamental gaps in our understanding of their physical processes, how these change with time and space, and how this results in their high mobility and destructive potential. Numerical and analogue models aim to address this lack of understanding. They can simulate a range of physical processes at a range of scales, to varying degrees of complexity. Results from physics-based models can feed into the development of data-driven hazard models that simulate PDC inundation during volcanic eruptions. This in turn will transform future risk and impact analysis for communities living with volcanic hazards. Since the hostile interiors of active PDCs have been inaccessible to direct observation, creation of new laboratory-, field-, and remote-based instruments through multinational and multi-instrument efforts would be transformational in probing the internal properties of real-world PDCs.

Main references

[1] Brown, S.K., Jenkins, S.F., Sparks, R.S.J., Odbert, H., Auker, M.R., 2017. Volcanic fatalities database: analysis of volcanic threat with distance and victim classification. *J. Appl. Volcanol.*, 6:15. <https://doi.org/10.1186/s13617-017-0067-4>.

- 675 [2] Giordano, G., Cas, R., Wright, J. V., 2024. Subaerial Pyroclastic Density Currents (Pyroclastic Flows
676 and Surges) Origins, Types, and Deposit Characteristics. In *Volcanology: Processes, Deposits, Geology
677 and Resources* (pp. 693-889). Cham: Springer International Publishing.
- 678 [3] Branney, M.J., Kokelaar, P., 2002. Pyroclastic density currents and the sedimentation of ignimbrites.
679 *Geological Society Memoir*, No. 27.
- 680 [4] Lube, G., Breard, E.C.P., Esposti Ongaro, T., Dufek, J., Brand, B., 2020. Multiphase flow behaviour and
681 hazard prediction of pyroclastic density currents. *Nat. Rev. Earth Environ.*, 1:348–365.
682 <https://doi.org/10.1038/s43017-020-0064-8>
- 683 [5] Dufek, J., 2016. The Fluid Mechanics of Pyroclastic Density Currents. *Annu. Rev. Fluid Mech.*, 48:459–
684 485. <https://doi.org/10.1146/annurev-fluid-122414-034252>
- 685 [6] Iverson, R. M., 2005. Regulation of landslide motion by dilatancy and pore pressure feedback. *J.
686 Geophys. Res. Earth Surf.*, 110.
- 687 [7] Valentine, G.A., 2020. Initiation of dilute and concentrated pyroclastic currents from collapsing mixtures
688 and origin of their proximal deposits. *Bull. Volcanol.*, 82:20. <https://doi.org/10.1007/s00445-00020-01366-x>
- 689 [8] Breard, E.C.P., Dufek, J., Charbonnier, S., Gueugneau, V., Giachetti, T., Walsh, B., 2023. The
690 fragmentation-induced fluidisation of pyroclastic density currents. *Nat. Commun.* 14, 2079.
691 <https://doi.org/10.1038/s41467-023-37867-1>.
- 692 [9] Lerner, G.A., Jenkins, S.F., Charbonnier, S.J., Komorowski, J.-C., Baxter, P.J., 2022. The hazards of
693 unconfined pyroclastic density currents: A new synthesis and classification according to their deposits,
694 dynamics, and thermal and impact characteristics. *J. Volcanol. Geotherm. Res.*,
695 <https://doi.org/10.1016/j.jvolgeores.2021.107429>
- 696 [10] Charbonnier, S.J., Garin, F., Rodríguez, L.A., Ayala, K., Cancel, S., Escobar-Wolf, R., Chigna, G.,
697 Chun-Quinillo, C., González, D., Chigna, W., Chun-Quinillo, K., Mérida, R., Juárez, F., Calder, E.S., 2023.
698 Unravelling the dynamics and hazards of the June 3rd, 2018, pyroclastic density currents at Fuego volcano
699 (Guatemala), *J. Volcanol. Geotherm. Res.*, 436, 10779. <https://doi.org/10.1016/j.jvolgeores.2023.107791>
- 700 [11] Bursik, M.I., Woods, A.W., 1996. The dynamics and thermodynamics of large ash-flows. *Bull. Volcanol.*,
701 58, 175–193.
- 702 [12] Roche, O., Azzaoui, N., Guillin, A., 2021. Discharge rate of explosive volcanic eruption controls runout
703 distance of pyroclastic density currents: *Earth and Planetary Science Letters*, v. 568,
704 <https://doi.org/10.1016/j.epsl.2021.117017>.
- 705 [13] Belousov, A., Voight, B., Belousova, M., 2007. Directed blasts and blast-currents: a comparison of the
706 Bezymianny 1956, Mount St Helens 1980, and Soufriere Hills, Montserrat 1997 eruptions and deposits.
707 *Bull. Volcanol.*, 69: 701-740.
- 708 [14] Brand, B. D., Pollock, N., Vallance, J. W., Ongaro, T. E., Roche, O., Trolese, M., Giordano, G., Marshall,
709 A.A., Criswell, C. W., 2023. Advances in our understanding of pyroclastic current behavior from the 1980
710 eruption sequence of Mount St. Helens volcano (Washington), USA. *Bull. Volcanol.*, 85(4), 24.

[15] Pollock, N.M., Brand, B.D., Rowley, P.J., Sarocchi, D., Sulpizio, R., 2019. Inferring pyroclastic density current flow conditions using syn-depositional sedimentary structures. *Bull. Volcanol.*, 81, 46. <https://doi.org/10.1007/s00445-019-1303-z>

[16] Dellino, P., Dioguardi, F., Rinaldi, A., Sulpizio, R., Mele, D., 2021. Inverting sediment bedforms for evaluating the hazard of dilute pyroclastic density currents in the field. *Scientific Reports*, 11(1), p.21024.

[17] Esposti Ongaro, T., Cerminara, M., Charbonnier, S.J., Lube, G., Valentine, G.A., 2020b. A framework for validation and benchmarking of pyroclastic current models. *Bull. Volcanol.*, 82:51. <https://doi.org/10.1007/s00445-020-01388-2>

[18] Lube, G., Breard, E.C.P., Cronin, S.J., Jones, J., 2015. Synthesizing large-scale pyroclastic flows: Experimental design, scaling, and first results from PELE, *J. Geophys. Res. Solid Earth*, 120, 1487–1502, [doi:10.1002/2014JB011666](https://doi.org/10.1002/2014JB011666).

[19] Gueugneau, V., Charbonnier, S., Roche, O., 2022. PyroCLAST: a new experimental framework to investigate overspilling of channelized, concentrated pyroclastic currents. *Bull. Volcanol.*, 85:5. <https://doi.org/10.1007/s00445-022-01623-y>

References to other Encyclopedia of Volcanoes chapters:

[E1] Dufek, J., Esposti Ongaro, T., Roche, O., 2015. Pyroclastic Density Currents: Processes and Models. In: *The Encyclopedia of Volcanoes*, 2nd edn., Elsevier Inc, pp. 617-629.

[E2] C. Harnett et al., Lava domes and coulées, in : C. Bonnadonna et al. (Eds.), Part 3, Chapter 3.2.

[E3] M. Cassidy et al., Hybrid eruptions: simultaneous dome - plumes/PDCs, in : C. Bonnadonna et al. (Eds.), Part 3, Chapter 2.5.

[E4] P. Cole et al., Impacts of pyroclastic density currents, in : C. Bonnadonna et al. (Eds.), Part 4, Chapter 2.3.

Figure references:

[F1] Capecelatro, J., Desjardins, O., 2023. Volume-filtered Euler–Lagrange method for strongly coupled fluid–particle flows. *Modeling Approaches and Computational Methods for Particle-Laden Turbulent Flows*, Academic Press, 383-417.

[F2] Andrews, B.J., Manga, M., 2012. Experimental study of turbulence, sedimentation, and coignimbrite mass partitioning in dilute pyroclastic density currents. *J. Volcanol. Geotherm. Res.*, 225–226:30–44. <https://doi.org/10.1016/j.jvolgeores.2012.02.011>

[F3] Breard, E.C.P., Lube, G., 2017. Inside pyroclastic density currents – uncovering the enigmatic flow structure and transport behaviour in large-scale experiments. *Earth Planet. Sci. Lett.*, 458:22–36. <https://doi.org/10.1016/j.epsl.2016.10.016>

[F4] Dellino, P., Zimanowski, B., Büttner, R., La Volpe, L., Mele, D., Sulpizio, R., 2007. Large-scale experiments on the mechanics of pyroclastic flows: Design, engineering, and first results, J. Geophys. Res., 112, B04202, doi:10.1029/2006JB004313.

[F5] Roche, O., 2012. Depositional processes and gas pore pressure in pyroclastic flows: an experimental perspective. Bull. Volcanol., 74:1807–1820. <https://doi.org/10.1007/s00445-012-0639-4>

[F6] Sulpizio, R., Castioni, D., Rodriguez-Sedano, L.A., Sarocchi, D., Lucchi, F., 2016. The influence of slope-angle ratio on the dynamics of granular flows: insights from laboratory experiments. Bull Volcanol 78:77. <https://doi.org/10.1007/s00445-016-1069-5>

[F7] Charbonnier, S., Gertisser, R., 2011. Deposit architecture and dynamics of the 2006 block-and-ash flows of Merapi Volcano, Java, Indonesia. Sedimentology 58, 1573–1612.

[F8] Charbonnier, S.J., Germa, A., Connor, C.B., Gertisser, R., Preece, K., Komorowski, J-C., Lavigne, F., Dixon, T., Connor, L., 2013. Evaluation of the impact of the 2010 pyroclastic density currents at Merapi volcano from high-resolution satellite imagery, field investigations and numerical simulations. J. Volcanol. Geotherm. Res., 261:295–315. <https://doi.org/10.1016/j.jvolgeores.2012.12.021>

[F9] Breard, E.C.P., Lube, G., Cronin, S.J., Fitzgerald, R., Kennedy, B., Scheu, B., Montanaro, C., White, J.D.L., Tost, M., Procter, J.N. and Moebis, A., 2014. Using the spatial distribution and lithology of ballistic blocks to interpret eruption sequence and dynamics: August 6 2012 Upper Te Maari eruption, New Zealand. J. Volcanol. Geotherm. Res., 286, 373-386.

Further reading:

Please add QR6 code for Further reading: Miscellaneous' here

Disclaimer:

"Any use of trade, firm, or product names is for descriptive purposes only and does not imply endorsement by the U.S. Government."